Combining Sonodynamic Therapy with Chemoradiation for the Treatment of Pancreatic Cancer

Richard J Browning[1], Sarah Able[1], Jia-Ling Ruan[1], Luca Bau[2], Phillip D Allen[1], Veerle Kersemans[1], Sheena Wallington[1], Paul Kinchesh[1], Sean Smart[1], Christiana Kartsonaki[3], Sukanta Kamila[4], Keiran Logan[4], Mark A Taylor[5], Anthony P McHale[4*], John F Callan[4*], Eleanor Stride[2*] and Katherine A Vallis[1*].

[1] Oxford Institute for Radiation Oncology, Department of Oncology, University of Oxford, Oxford, UK, OX3 7DQ
[2] Department of Engineering Science, University of Oxford, Oxford, UK, OX3 7DQ
[3] MRC Population Health Research Unit, Clinical Trials Service Unit and Epidemiological Studies Unit (CTSU), Nuffield Department of Population Health, University of Oxford, Oxford, UK, OX3 7DQ
[4] Biomedical Sciences Research Institute, University of Ulster, Coleraine, Northern Ireland, U.K. BT52 1SA
[5] Department of HPB Surgery, Mater Hospital, Belfast, Northern Ireland, U.K. BT14 6AB

* Principal Investigators of equal contribution

Running Title: Combining chemoradiotherapy and SDT for Pancreatic Cancer

Keywords: Sonodynamic therapy, chemoradiotherapy, pancreatic cancer, ultrasound, oxygen microbubbles.

Additional information: RJB was supported through a Pancreatic Cancer Research Fund grant. KAV and SA acknowledge support from Cancer Research-UK (C5255/A15935). KAV, PDA, VK, SW, PK, and SS received funding through the CRUK/EPSRC Cancer Imaging Centre Oxford (C5255/A16466). KAV and ES acknowledge support from the EPSRC Oxford Centre for Drug Delivery Devices (EP/L024012/1).

Corresponding author: Prof. Katherine Vallis
Oxford Institute for Radiation Oncology, Old Road Campus Research Building,
Oxford, OX3 7DQ, UK
+44 (0)1865 225209; katherine.vallis@oncology.ox.ac.uk

The authors declare no conflicts of interest.
Word count: 5944
Number Figures and Tables: 5 figures (Supplementary Information: 5 figures)

Abstract

Treatment options for patients with pancreatic cancer are limited and survival prospects have barely changed over the past 4 decades. Chemoradiation treatment (CRT) has been used as neoadjuvant therapy in patients with borderline resectable disease to reduce tumour burden and increase the proportion of patients eligible for surgery. Antimetabolite drugs such as gemcitabine and 5-fluorouracil are known to sensitise pancreatic tumours to radiation treatment. Likewise, photodynamic therapy (PDT) has also been shown to enhance the effect of radiation therapy. However, PDT is limited to treating superficial lesions due to the attenuation of light by tissue. The ability of the related technique, sonodynamic therapy (SDT), to enhance CRT was investigated in two murine models of pancreatic cancer (PSN-1 and BxPC-3) in this study. SDT uses low intensity ultrasound to activate an otherwise non-toxic sensitiser, generating toxic levels of reactive oxygen species (ROS) locally. It is applicable to greater target depths than PDT due to the ability of ultrasound to propagate further than light in tissue. Both CRT and the combination of CRT plus SDT delayed tumour growth in the two tumour models. In the PSN-1 model, but not the BxPC-3 model, the combination treatment caused an increase in survival relative to CRT alone ($p = 0.038$). The improvement in survival conferred by the addition of SDT in this model may be related to differences in tumour architecture between the two models. MRI and US images showed that PSN-1 tumours were less well perfused and vascularised than BxPC-3 tumours. This poor vascularisation may explain why PSN-1 tumours were more susceptible to the effects of vascular damage exerted by SDT treatment.

1. Introduction

Pancreatic cancer is usually diagnosed at an advanced stage with only 20% of patients being eligible for surgery [1]. A further 30% of patients present with locally advanced or borderline resectable pancreatic cancer (BRPC) and 50% present with metastatic disease [2]. For those patients with BRPC, neoadjuvant therapy can be used to downstage the tumour and improve eligibility for surgical resection [3]. This is particularly important as surgery remains the only curative treatment for pancreatic cancer and is associated with a 5-fold improvement in the 5-year survival rate [4, 5]. Current neoadjuvant approaches involve either chemotherapy alone or in combination with radiotherapy (termed chemoradiation therapy, CRT) [6]. Gemcitabine, an anti-metabolite chemotherapy, is widely used in the treatment of pancreatic cancer and is often combined with external beam radiation therapy (EBRT) in CRT protocols [7] due to its ability to act as a radiosensitiser. The di-phosphorylated analogue of gemcitabine (dFdCDP) inhibits ribonucleotide reductase, resulting in depletion of cellular deoxynucleotide triphosphate pools. This is thought to be one of the mechanisms by which it radiosensitises cells [8, 9].

Previous pre-clinical work in pancreatic cancer has demonstrated that antimetabolite chemotherapy also combines very effectively with sonodynamic therapy (SDT) [10, 11]. SDT involves the administration of a relatively non-toxic compound to cells that sensitises the cells to simultaneous or subsequent ultrasound exposure. The combination of the sonosensitiser and ultrasound leads to the generation of reactive oxygen species (ROS) that causes cellular death via oxidative stress [12]. To target delivery of the SDT sonosensitiser and antimetabolite more precisely to pancreatic tumours, we have attached these compounds to the shell of ultrasound-responsive phospholipid-stabilised microbubbles [10, 11]. Microbubbles are currently approved as contrast agents for diagnostic ultrasound imaging and have also been investigated as drug delivery vectors [13-16]. When exposed to ultrasound of sufficient intensity, the microbubbles undergo inertial cavitation (i.e. collapse) producing a range of therapeutically relevant effects [17, 18]. As ultrasound can be tightly focussed in 3 dimensions in human tissue, these effects can be confined to the target site. In the context of SDT, a key

effect is the generation of light by the collapsing bubbles [19] which activates the sensitiser. In addition, the motion of the surrounding liquid induced by the bubble oscillations can enhance dispersion of the drugs into the tumour tissue [20, 21].

Our motivation for combining CRT with SDT is driven by previous reports of a therapeutic benefit afforded by the combination of radiotherapy and photodynamic therapy (PDT) [22, 23]. PDT is a clinically approved treatment that is similar to SDT but uses light instead of ultrasound to activate a sensitiser drug [24]. A major limitation of PDT that has restricted its more widespread clinical use is the inability of light to penetrate deeply into human tissue. This obstacle is overcome in SDT as the low-intensity ultrasound used for sensitiser activation can penetrate tens of centimetres into human tissue. Therefore, in addition to the beneficial therapeutic effect of combining SDT and antimetabolite chemotherapy, we hypothesise that SDT may also compliment chemoradiotherapy. As SDT is a targeted treatment, any therapeutic advantage obtained should not be at the cost of off-target toxicity.

In this study, we investigate the effect of combining CRT with SDT using gemcitabine as a radiosensitiser in two subcutaneous murine models of human pancreatic cancer. We determine the therapeutic advantage obtained by combining CRT with SDT and investigate the importance of tumour architecture in determining treatment efficacy.

2. Materials and Methods

2.1 Reagents

The lipids 1,2-dibehenoyl-sn-glycero-3-phosphocholine (DBPC), 1,2-distearoyl-sn-glycero-3-phosphoethanolamine-N-[methoxy(polyethyleneglycol)-2000] (DSPE-PEG(2000)) and 1,2-distearoyl-sn-glycero-3-phosphoethanolamine-N-[biotinyl(polyethylene glycol)-2000] (DSPE-PEG(2000)-biotin) were purchased from Avanti Polar Lipids. Oxygen (O_2) was purchased from BOC Industrial Gases. Decafluorobutane (perfluorobutane, PFB) was purchased from FluoroMed LP. Matrigel was purchased from Corning. Biotinylated Rose Bengal (bRB) was prepared using a previously described method [25]. PSN-1 and BxPC-3, human pancreatic

adenocarcinoma cell lines, were purchased from American Type Culture Collection (ATCC). Cells were cultured in RPMI-1640 medium supplemented with 10% FBS, 120 units/mL Penicillin, 100 µg/mL Streptomycin and 2 mM L- glutamine. All cells were used at less than 10 passages from stock. Cells were tested regularly and found to be mycoplasma-free. Cells were authenticated by ATCC before implanting into mice. Cells were counted using a Countess II Cell counter (Thermo Fisher Scientific). All other chemicals were purchased from Sigma Aldrich or Thermo Fisher Scientific unless otherwise stated.

2.2 Manufacture of sonosensitiser (Rose Bengal)-loaded oxygen microbubbles

DBPC, DSPE-PEG(2000) and DSPE-PEG(2000)-biotin were prepared as 25 mg/mL solutions in chloroform, mixed at a molar ratio of 82:9:9 (7.2 mg total lipid amount) and the solvent evaporated on a hotplate at 50^{o}C overnight. The resulting film was reconstituted in an 8:1:1 v:v solution (2 mL) of sterile PBS:glycerol:propylene glycol (PGP) and stirred at 100^{o}C on a hotplate for 30-60 min followed by sonication (20%, Qsonica Q125) for 90s to fully disperse the lipids. The sonicator horn was then moved to the liquid-air interface and the headspace filled with perfluorobutane (PFB) gas. Under continuous PFB flow, the solution was sonicated (80%, Qsonica Q125) for 20s to generate the microbubble (MB) suspension. Avidin (500 µL, 10 mg/mL in PGP) was added to the MB suspension and stirred on ice for 5 minutes. Excess avidin was removed by centrifugation at 300g for 5 min at 4^{o}C, and the resulting infranatant was discarded. The microbubble cake was resuspended in 1 mL of PGP solution. Rose Bengal, a sonosenitiser, was prepared as a biotinylated (bRB) solution by adding bRB (4 mg) to 150 µL of dimethylsulfoxide (DMSO) and warmed until fully dissolved. This was then diluted to 1 mL total volume with a sterile-filtered solution of PGP solution. This was then sterile filtered through a 0.2 µm nylon filter to remove precipitates. The concentration was measured by preparing a standard curve using the unfiltered bRB solution and measuring absorbance at 560 nm using a plate spectrophotometer (FLUOstar Omega, BMG Labtech). Filtered bRB solution was added to a volume of microbubbles to yield a suspension containing 5 x 10^{8} MB/mL and 500 µM bRB. The vial was then sparged with oxygen for 2 minutes. The final

product, RB-O_2MB, was protected from light and sealed with a rubber septum for use on the same day as manufacture. Optical imaging of the MBs showed spherical particles with an average diameter of 1-2 µm.

2.3 In vivo tumour models

Animal procedures were performed in accordance with the UK Animals (Scientific Procedures) Act 1986 and with local Animal Welfare and Ethical Review Body approval. Mice were housed in individually ventilated cages with *ad libitum* access to water and food. Female, Crl:NU(NCr)-Foxn1nu mice (athymic nude) were purchased from Charles River or Envigo and entered the study at 8-10 weeks of age. Mice were assigned to treatment groups prior to implantation to avoid bias. Tumour cells were implanted under brief isoflurane anaesthesia. 2 x 10^6 cells (PSN-1) or 1 x 10^7 cells (BxPC-3) in a 50:50 v:v mixture of Matrigel:serum-free medium (100 µL) were implanted in the rear right flank of the animals using a 30G insulin syringe. In the therapy study (see schema in **Figure 1** and Section 2.6 below) tumour volume was measured using calipers once every two days for PSN-1 tumours and once every three days for BxPC-3 tumours. Three dimensions of the tumour were measured and the volume (V) calculated as V=(LxWxH)/2. Animals were entered into the treatment protocol when tumours reached 90 to 150 mm^3 (PSN-1) or 190 to 250 mm^3 (BxPC-3) as preliminary data (not shown) had demonstrated that these tumour volume ranges were the starting point of exponential growth. A separate cohort of tumour bearing mice were entered into an imaging study (see Section 2.4).

2.4 MRI and US characterisation of tumours

Animals bearing PSN-1 or BxPC-3 tumours were imaged longitudinally at timepoints following tumour implantation using dynamic contrast enhanced MRI (DCE-MRI) and contrast enhanced ultrasound (CEUS). Imaging was conducted under isoflurane anaesthesia. Animals were prepared by applying eye lubricant to the surface of both eyes and administering a subcutaneous sterile saline injection for fluid maintenance during the procedure. A 30G

cannula was placed in the tail vein and secured using skin glue and micropore tape. Mice were first imaged by CEUS, then DCE-MRI. For CEUS, animals were imaged using VisualSonics Vevo 3100 (FUJIFILM VisualSonics Inc) with the ultrasound contrast agent SonoVue (Bracco UK Ltd), prepared following the manufacturer's instructions. During imaging, SonoVue was kept on ice to reduce degradation of microbubbles over time. The mice were positioned on a heated stage and the subcutaneous tumour visually located under the imaging transducer probe mounted on the automated 3D stage, and confirmed by VevoLab image software. Skin was taped taut to reduce excess motion during 3D acquisition. The temperature of the animals was monitored throughout the session using a rectal thermometer, and the respiration rate monitored using a pressure balloon. The body temperature was maintained at above 35ºC throughout the session. Two ultrasound imaging scans were performed: 1) a 3D scan of tumour for measurement of volume. Next, a tumour slice with detectable vascularity around the tumour centre was located using power doppler and the probe fixed in position. If power doppler did not reveal a region of high vascularity, the probe was positioned approximately at the tumour centre. At this position, in contrast mode, 2) a perfusion CEUS video was taken with a 50 µL bolus of SonoVue injected 8 seconds after time 0. Imaging continued for approximately 50 seconds to capture bolus perfusion. After imaging, ultrasound burst pulses were applied to the region to destroy any remaining contrast agent. The mouse was then prepared for DCE-MRI while maintained under anaesthesia.

Dynamic contrast enhanced (DCE) MRI was performed at 7 T (VNMRS, Varian Inc) using a 32 mm diameter quadrature birdcage coil (Rapid Biomedical GmbH) for transmission and signal detection. Animals were positioned in a custom-made cradle that incorporated tooth-bar positioning, respiratory monitoring via a pressure balloon and MR-compatible electrical heating [26]. The body temperature was maintained at above 35ºC throughout the session. A respiratory-gated 3D FLASH scan incorporating dynamic reacquisition was used with TE = 0.7 ms, TR = 1.6 ms, bandwidth = 100 kHz, FOV = 64x32x32 mm and matrix = 128x64x64 image points [27]. T1 was estimated using the variable flip angle (VFA) approach with B1 transmission inhomogeneities corrected using a respiratory gated implementation of

the Actual Flip Angle (AFA) imaging scan incorporating dynamic reacquisition and operated at TE = 0.6 ms, TR = 10,100 ms, FOV = 64x32x32 mm and matrix = 64x32x32 image points [28]. T1 was calculated from the VFA and AFA images using a non-linear least squares fitting with a calculation time of approximately 6 seconds [29]. The Gadolinium uptake scan was performed using scan parameters as for the VFA acquisition but at a fixed flip angle of 5 degrees, and with 30 μL of contrast agent (Omniscan, GE Healthcare) infused by syringe pump (PHD2000, Harvard Apparatus) over 5 seconds and starting under scanner control at the beginning of scan repeat 11/50. Details of the analysis of the DCE-MRI data is given in the Supplementary Information. Imaging sessions lasted a maximum of 2 h in total. There was variation in the number of imaging episodes per mouse: there was one case of anaesthetic death in the MRI group, one mouse was euthanised early due to tumour ulceration, and a few measurements were missed due to slow recovery of the mouse following the previous anaesthetic/imaging session (as indicated by weight loss). A few mice were euthanised before the final imaging session to harvest tumours to develop immunostaining protocols for markers of interest for future experiments. After imaging was complete, animals were recovered on a half-heated mat to allow for thermoregulation, with access to water and moist food.

2.5 Treatment of mice bearing PSN-1 tumours with gemcitabine or EBRT as single agents or with CRT (gemcitabine and EBRT)

A preliminary experiment to determine the effect of gemcitabine alone, EBRT alone or gemcitabine plus EBRT (CRT) in the absence of SDT was conducted in mice bearing PSN-1 xenografts. A control group of untreated mice were included. Gemcitabine was prepared as a solution of gemcitabine hydrochloride in PBS, adjusted to a neutral pH with sodium hydroxide, and administered at 120 mg/kg by intraperitoneal (i.p.) injection; this dose was selected as we have shown previously that it is well-tolerated albeit in a different mouse strain [11]. EBRT was delivered under isoflurane anaesthesia. Animals were covered with a lead shield ensuring only

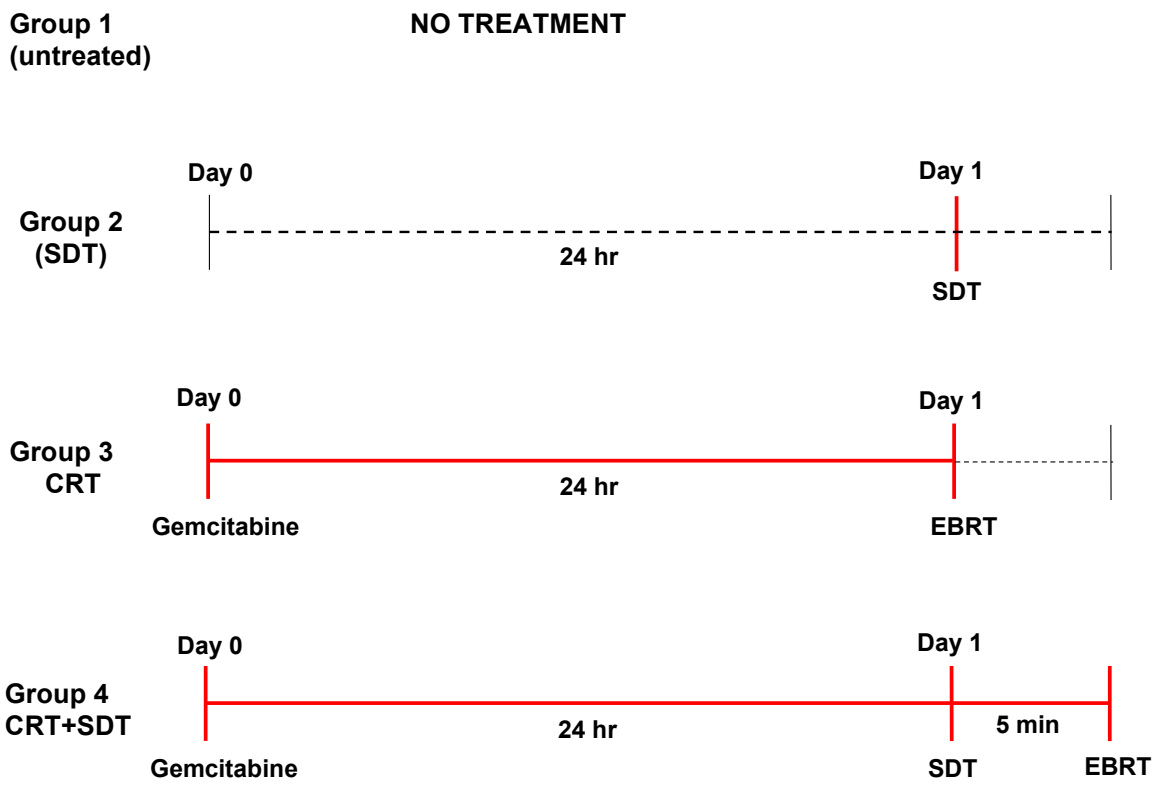

Figure 1. Schematic of the treatment protocol

the tumour was exposed. The animal was then positioned in a Xstrahl/Gulmay RS320 irradiator (Xstrahl Ltd) and 300 kV X-irradiation delivered at approximately 2.26 Gy/min for a total of 4 Gy, a dose which was shown in preliminary studies to cause minor tumour growth delay but which, as a single treatment, did not eliminate tumour growth all together. During irradiation the breathing rate was monitored using a pressure balloon. For the CRT group, animals were treated with gemcitabine and EBRT was administered 24 h later. Following treatment, tumour volume was recorded until a volume of approximately 500 mm^3 was reached, when mice were euthanised using a Schedule 1 method.

2.6 Treatment of mice bearing PSN-1 and BxPC-3 tumours with CRT plus SDT

To investigate the effect of SDT when combined with CRT, four treatment groups were set up (**Figure 1**). Group 1 received no treatment. Group 2 received SDT only. Group 3 received gemcitabine plus EBRT (CRT); on day 0, animals were treated with gemcitabine and EBRT

was administered 24 h later. Group 4 received gemcitabine, EBRT and SDT (CRT + SDT); on day 0, animals were treated with gemcitabine, followed 24 h later by SDT, followed 5 min later by EBRT. Gemcitabine was prepared as described above. In the PSN-1 experiments, gemcitabine was administered at 120 mg/kg by intraperitoneal (i.p.) injection. However, due to evidence of toxicity (decrease in body weight up to 15%) observed at this concentration, the concentration was lowered to 100 mg/kg in the subsequent experiment using the BxPC-3 model. SDT treatment was carried out under isoflurane anaesthesia. The RB-O_2MB suspension (100 µL) was injected intravenously (i.v.) using a 30G insulin syringe via a 30G tail-vein catheter. A total of 5 x 10^7 MBs and 0.5 µmol RB (2.5 – 3.0 mg/kg) were injected per treatment. This was immediately followed by ultrasound applied for 3.5 minutes to the tumours using a Sonidel SP100 sonoporator (Sonidel Ltd). Ultrasound settings were based on previous work and were: 1 MHz centre frequency, 30% duty cycle, 100 Hz pulse repetition frequency, at 3.5 W/cm^2 – measured as approximately 880 kPa (peak negative pressure) by a calibrated, 200 µm needle hydrophone (Precision Acoustics Ltd) at peak focus. For experiments using the PSN-1 tumour model, a single application of ultrasound was given, while for experiments using the BxPC-3 tumour model an additional application of ultrasound was given using the same settings 25 minutes after the injection of RB-O_2MB as done previously [11]. The rationale for two applications of US was that the first would burst the MB and activate SDT. The gap was to allow any released RB time to be taken up. The second US treatment was then delivered to activate SDT again. The effect of an additional ultrasound application for the PSN-1 model is detailed in Supplementary Information. EBRT (4 Gy) was delivered as described above. For Group 4 mice, SDT was applied first and mice were maintained under anaesthesia for application of EBRT.

2.7 Statistical analysis.

Mice were followed up from the time of treatment until their tumours reached a size of 500 mm^3 (PSN-1), or 600 mm^3 (BxPC-3) tumours, when they were euthanised. Mice that were euthanised before the tumour volumes reached these limits were censored at the time they

were euthanised. Kaplan–Meier curves for survival by treatment group were plotted. Survival was compared between groups by fitting a log-normal model. Tumour growth data were analysed by fitting a (multilevel) linear regression model with the logarithm of tumour volume as the outcome. To assess how the relationship of enhancing fraction and highly enhancing fraction (MRI) with tumour volume varies by cell line a (multilevel) linear regression model was fitted. To assess whether the relationship of maximum intensity (ultrasound) with tumour volume varies by cell line a (multilevel) linear regression model was fitted. Analysis was done using R version 4.0.22 [30] and full details are reported in Supplementary Information.

3. Results and Discussion

A pilot study was conducted to evaluate the *in vivo* effect of gemcitabine alone, EBRT alone or gemcitabine plus EBRT (CRT) in the absence of SDT in the PSN-1 tumour model (**Figure S1**). Analysis of tumour growth data revealed that gemcitabine used alone or in combination with EBRT significantly reduced the rate of tumour growth ($p<0.001$ for both treatment groups compared to untreated animals) (**Figure S1a**). However, mice showed greater survival compared to the untreated animals only in the CRT group ($p=0.0012$) (**Figure S1b**). Next, the effect of SDT alone, CRT alone and CRT + SDT on tumour growth and survival were investigated in the PSN-1 tumour model (**Figure 2**). Linear regression analysis of the tumour growth curves revealed that CRT alone and the combination of CRT + SDT both significantly reduced the rate of tumour growth for both treatment groups compared to untreated animals ($p<0.001$). However, the CRT + SDT treatment did not slow tumour growth statistically significantly compared to CRT alone ($p=0.22$). Analysis of survival data revealed that animals in both the CRT alone and the combination treatment group survived longer compared to untreated animals ($p=0.0064$ and $p<0.001$, respectively). This analysis also showed that animals in the CRT + SDT treatment group had improved overall survival compared to animals that received CRT alone ($p=0.038$). One animal in the combination group survived 66 days post-treatment and was ultimately euthanised due to age rather than tumour burden. The

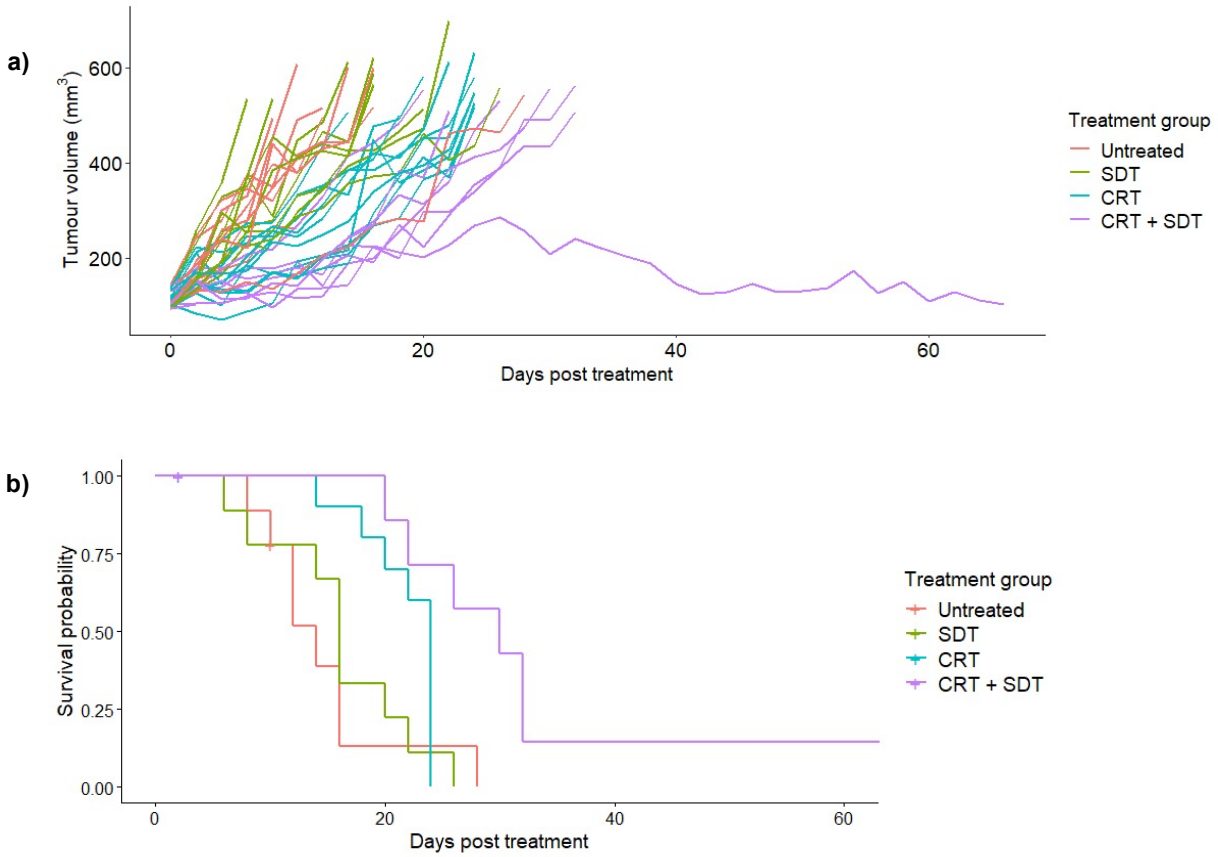

Figure 2. (a) Individual tumour growth curves and (b) Kaplan-Meier curve for PSN-1 tumour bearing mice that were either untreated (n=8) or treated with SDT alone (n=9), CRT alone (n=10), or CRT + SDT (n=7).

influence of this animal on the survival comparisons in the PSN-1 therapy experiment was tested by censoring it at 32 days (the timepoint at which the next longest surviving animal, also from the CRT + SDT group, reached tumour volume of 500 mm^3 and was euthanised). With removal of the long-term surviving mouse from the analysis at 32 days the difference in overall survival for the two groups, CRT + SDT versus CRT, is weaker (p=0.19, compared to p=0.038 without censoring). The observation that the tumour of the "cured mouse" grew with similar kinetics to other tumours in the group during the early post-treatment phase (first 18 days) indicates that this was a true response to CRT + SDT. A similar therapy study was also carried out using the BxPC-3 tumour model (**Figure 3**). In this case, two ultrasound doses were applied during SDT treatment to provide consistency with recent published data for this model [11]. A preliminary experiment was performed to determine the effect of two applications of ultrasound versus a single exposure on SDT-mediated tumour growth delay (**Figure S2**

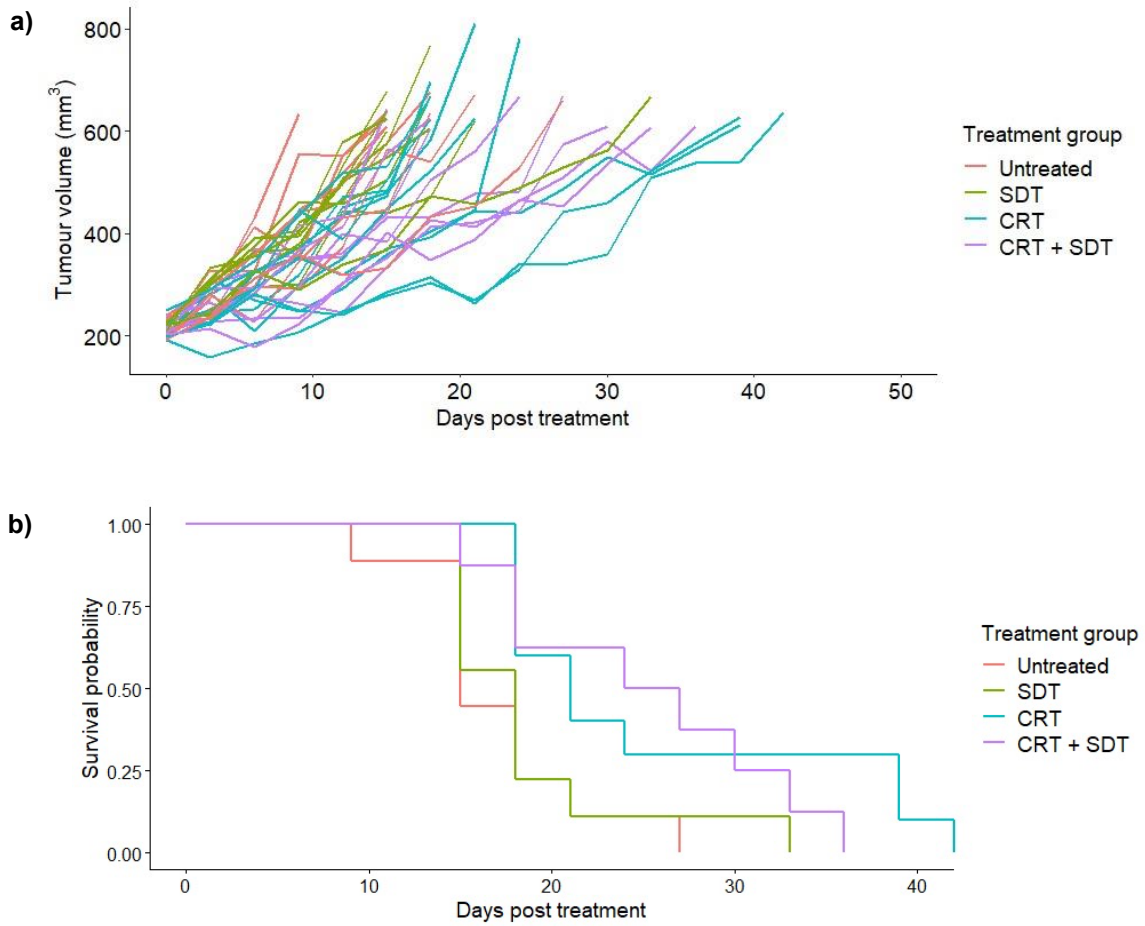

Figure 3. (a) Individual tumour growth curves and (b) Kaplan-Meier curve for BxPC-3 tumour bearing mice which were either untreated (n=9) or treated with SDT alone (n=9), CRT alone (n=10), or SDT + CRT (n=8).

shows the experimental schema). For expediency, this experiment was performed in the faster-growing PSN-1 model. The experiment showed that SDT alone did not cause a delay in tumour growth or alter survival when either a single or two applications of ultrasound were employed (**Figure S3**).

In the BxPC-3 model, analysis of the tumour growth curves (**Figure 3a**) revealed that, as for the PSN-1 model, both CRT alone and CRT + SDT significantly reduced the rate of tumour growth compared to untreated animals (p=0.004 and p=0.0146 respectively). Analysis of the survival data (**Figure 3b**) showed that animals in both the CRT alone and the combination treatment groups survived longer compared to untreated animals (p=0.0035 and p=0.0069 respectively). However, in contrast to the PSN-1 model, the combination treatment conferred no statistically significant survival advantage over CRT alone (p=0.753).

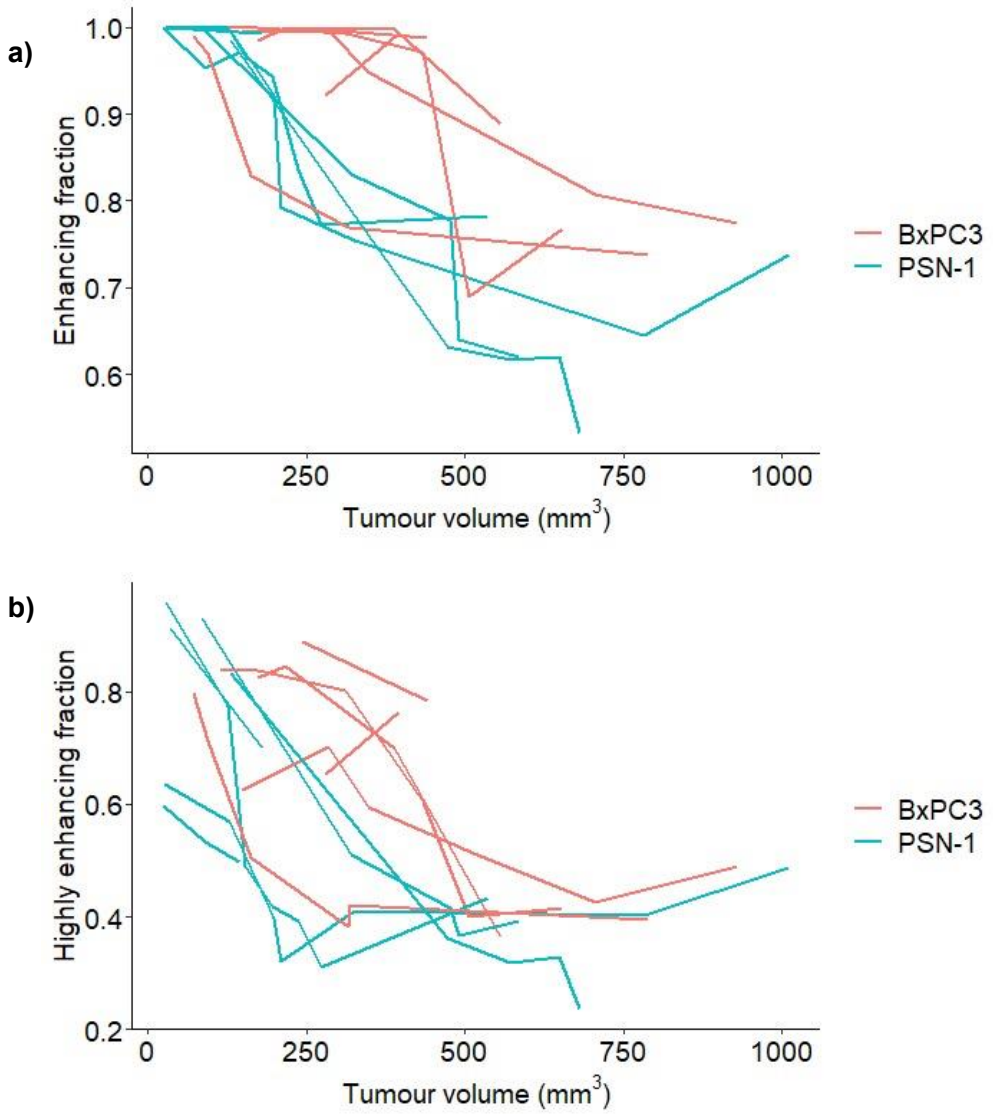

Figure 4. (a) Enhancing fraction and (b) Highly enhancing fraction for DCE-MRI analysis of PSN-1 and BxPC-3 tumours. Tumour volume was measured using MRI. Each line shows the results from a single mouse/tumour over time.

285 The results indicate that the addition of SDT treatment conferred an advantage over CRT
286 treatment in the PSN-1 but not the BxPC-3 model. This observation could be related to the
287 difference in growth rate between the two models, with PSN-1 tumours reaching the size at
288 which exponential growth commenced (treatment size) at 17 days ± 5 days following
289 implantation compared to 58 days ± 12 days for the BxPC-3 tumours. Faster dividing cells are
290 generally more susceptible to CRT [31-33]. DCE-MRI and CEUS were used to investigate how
291 this difference in growth rate may have influenced aspects of tumour architecture, particularly

tumour vascularisation. For MRI, the enhancing and highly enhancing fractions were measured in the tumours of animals bearing PSN-1 or BxPC-3 tumours over time (**Figure 4**). These parameters are measures of the distribution of the contrast agent (gadolinium) throughout the tumours. Gadolinium can distribute through tumours via perfusion through blood vessels, or the slower process of tissue diffusion. The enhancing fraction represents the percentage of the tumour that the gadolinium reached during the timeframe of the experiment, and as such, it encompasses both perfusion and diffusion. The highly enhancing fraction is derived from the initial rapid upstroke of the gadolinium signal in the tumours and is therefore more representative of the perfusion component. **Figure 4a** shows that BxPC-3 tumours generally have higher enhancing fractions compared to PSN-1 tumours, indicating the contrast agent reaches a greater proportion of the tumour. Linear regression analysis confirmed a significant difference in slope values for the two tumour models (p=0.0147) (**Figure S4a**). **Figure 4b** suggests a similar trend for the highly enhancing fraction, though this was not as clear, and there was no statistically significant difference in the slope values between tumour models (**Figure S4b**). The extent of contrast agent distribution throughout the tumours is illustrated pictorially in **Figure S5**. The BxPC-3 tumours have a greater proportion of perfused and enhancing voxels compared to PSN-1 tumours, which have a greater proportion of non-enhancing voxels, particularly at larger tumour volumes. Oxygen plays an important role in SDT and it is interesting to note that others have reported that DCE-MRI correlates well with the fraction of hypoxic tissue and microvessel density in human pancreatic cancer xenograft models including BxPC-3 [34]. Recent clinical studies have also shown that MRI is able to accurately characterize tumor collagen fraction, vessel density, and hypoxia in PDAC [35].

For CEUS data, the parameter measured was intensity of contrast agent signal within the tumour. **Figure 5** shows that the intensity of the contrast agent was greater in BxPC-3 tumours compared to PSN-1 tumours, though linear regression analysis showed no significant difference between the slopes for the two models (**Figure S4c**). In **Figure 4** the signal decreases with tumour volume. The enhancing fraction appears more dependent on tumour volume when measured by MRI compared to CEUS (**Figures 4 and 5**). The explanation for

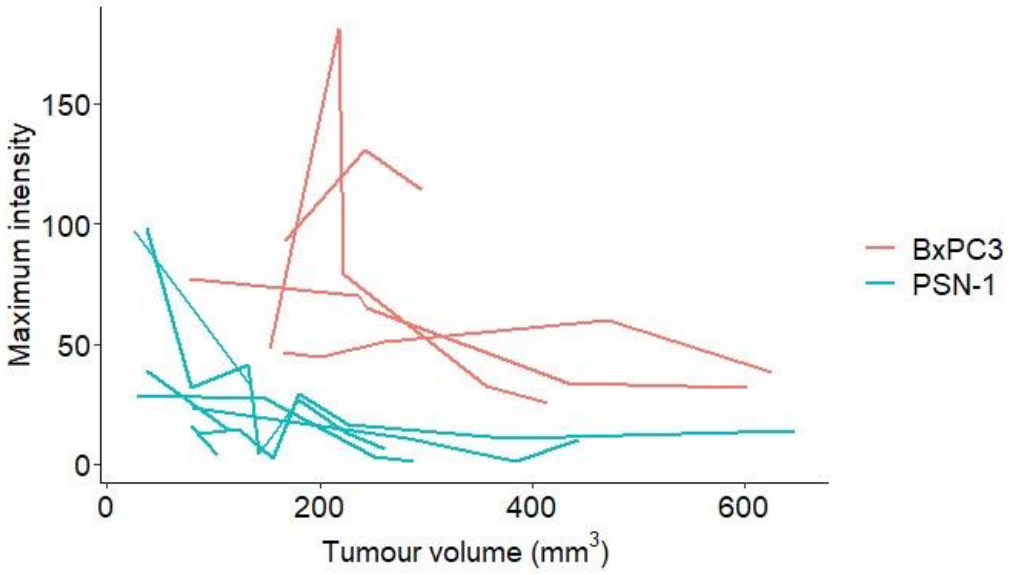

Figure 5. Maximum intensity from model fit of contrast enhanced ultrasound data. Tumour volume was measured by calliper. Each line shows the results from a single mouse/tumour over time.

this difference in the shape of the two sets of curves is that although MRI and CEUS both measure perfusion, the contrast agents used are hydrodynamically distinct as gadolinium is a small molecule and MB are large structures. Consequently, in leaky vasculature, the small molecule may be retained in tissue for longer. The MRI and CEUS analyses show that PSN-1 tumours are poorly perfused compared to BxPC-3 tumours, with vasculature largely confined to the periphery. BxPC-3 tumours appear to be vascularised throughout the tumour, which may result from their slow growth and delayed exponential growth period. Given the reduced and peripheral nature of perfusion associated with PSN-1 tumours, it is possible that they were more susceptible to SDT mediated vascular damage compared to BxPC-3 tumours. The immobilisation of Rose Bengal onto the microbubble surface and the inability of the resulting particles to extravasate the tumour vasculature until ultrasound mediated rupture would further target ROS generation to the tumour blood vessels. We postulate that this was the mechanism responsible for the increased survival benefit conferred by the addition of SDT to the treatment regimen in the PSN-1 model. It will be of interest to investigate the relationship between tumour response to CRT + SDT and perfusion although unfortunately it was not possible to do so in this study as the therapy and perfusion/imaging experiemnts were done separately,

using two different cohorts of mice. It is also interesting to note that BxPC-3 tumours which were exposed to US twice were less responsive to CRT + SDT than PSN-1 tumours which received only one exposure. Given this, it sems unlikely that the number of US exposures is a major determinant of the outcome of CRT + SDT. However, detailed investigation of this aspect of the CRT + SDT protocol merits further investigation. It is possible that increasing the number of SDT treatments given within a fixed time interval could provide additional benefit in terms of both tumour growth control and survival. Given that SDT is a targeted treatment with minimal off-target toxicity, the results from this study suggest that further exploration of its combination with CRT is merited.

4. Conclusion

SDT using ultrasound targeted microbubble destruction to enhance delivery of the Rose Bengal sonosensitiser, complemented CRT in the PSN-1 murine model of pancreatic cancer with significantly increased survival. The survival benefit of CRT + SDT was weak when a single apparently cured animal in the combined treatment group was censored early. The addition of SDT conferred no survival benefit compared to CRT alone in the BxPC-3 model. DCE-MRI and CEUS imaging indicated that BxPC-3 tumours are more extensively vascularised than PSN-1 and this, in combination with the slower growth rate of BxPC-3, may have influenced the treatment response of the two tumour models. The effect of varying the chemotherapy (gemcitabine) concentration and frequency of ultrasound applications in this set up require further investigation to understand their influence on the final outcome of CRT + SDT.

5. Acknowledgements

The authors acknowledge Professor Meng-Xing Tang and Dr Chee Hau Leow who assisted in analysing the CEUS data.

References

[1] G. Bond-Smith, N. Banga, T.M. Hammond, C.J. Imber, Pancreatic adenocarcinoma, British Medical Journal, 344 (2012) e2476.

[2] A. Soweid, The borderline resectable and locally advanced pancreatic ductal adenocarcinoma: Definition, Endoscopic Ultrasound, 6 (2017) 76-78.

[3] F. Scheufele, D. Hartmann, H. Friess, Treatment of pancreatic cancer—neoadjuvant treatment in borderline resectable/locally advanced pancreatic cancer, Transl. Gastroenterol. Hepatol., 4 (2019).

[4] S. Gillen, T. Schuster, C. Meyer zum Büschenfelde, H. Friess, J. Kleeff, Preoperative/Neoadjuvant Therapy in Pancreatic Cancer: A Systematic Review and Meta-analysis of Response and Resection Percentages, PLOS Medicine, 7 (2010) e1000267.

[5] D. O'Reilly, L. Fou, E. Hasler, J. Hawkins, S. O'Connell, F. Pelone, M. Callaway, F. Campbell, M. Capel, R. Charnley, P. Corrie, D. Elliot, L. Goodburn, A. Jewell, S. Joharchi, L. McGeeney, S. Mukherjee, K. Oppong, P. Whelan, J. Primrose, J. Neoptolemos, Diagnosis and management of pancreatic cancer in adults: A summary of guidelines from the UK National Institute for Health and Care Excellence, Pancreatology, 18 (2018) 962-970.

[6] T. Seufferlein, T.J. Ettrich, Treatment of pancreatic cancer-neoadjuvant treatment in resectable pancreatic cancer (PDAC), Transl. Gastroenterol. Hepatol., 4 (2019) 21.

[7] E. Versteijne, M. Suker, K. Groothuis, J.M. Akkermans-Vogelaar, M.G. Besselink, B.A. Bonsing, J. Buijsen, O.R. Busch, G.M. Creemers, R.M. van Dam, F. Eskens, S. Festen, J.W.B. de Groot, B. Groot Koerkamp, I.H. de Hingh, M.Y.V. Homs, J.E. van Hooft, E.D. Kerver, S.A.C. Luelmo, K.J. Neelis, J. Nuyttens, G. Paardekooper, G.A. Patijn, M.J.C. van der Sangen, J. de Vos-Geelen, J.W. Wilmink, A.H. Zwinderman, C.J. Punt, C.H. van Eijck, G. van Tienhoven, Preoperative Chemoradiotherapy Versus Immediate Surgery for Resectable and Borderline Resectable Pancreatic Cancer: Results of the Dutch Randomized Phase III PREOPANC Trial, J Clin Oncol, 38 (2020) 1763-1773.

[8] T.H. Doyle, F. Mornex, W.G. McKenna, The clinical implications of gemcitabine radiosensitization, Clin Cancer Res, 7 (2001) 226-228.

[9] D.S. Shewach, T.M. Hahn, E. Chang, L.W. Hertel, T.S. Lawrence, Metabolism of 2',2'-difluoro-2'-deoxycytidine and radiation sensitization of human colon carcinoma cells, Cancer Res, 54 (1994) 3218-3223.

[10] C. McEwan, S. Kamila, J. Owen, H. Nesbitt, B. Callan, M. Borden, N. Nomikou, R.A. Hamoudi, M.A. Taylor, E. Stride, A.P. McHale, J.F. Callan, Combined sonodynamic and antimetabolite therapy for the improved treatment of pancreatic cancer using oxygen loaded microbubbles as a delivery vehicle, Biomaterials, 80 (2016) 20-32.

[11] H. Nesbitt, Y. Sheng, S. Kamila, K. Logan, K. Thomas, B. Callan, M.A. Taylor, M. Love, D. O'Rourke, P. Kelly, E. Beguin, E. Stride, A.P. McHale, J.F. Callan, Gemcitabine loaded microbubbles for targeted chemo-sonodynamic therapy of pancreatic cancer, Journal of Controlled Release, 279 (2018) 8-16.

[12] M. Lafond, S. Yoshizawa, S.I. Umemura, Sonodynamic therapy: Advances and challenges in clinical translation, J. Ultrasound Med., 38 (2019) 567-580.

[13] E.C. Unger, T.P. McCreery, R.H. Sweitzer, V.E. Caldwell, Y. Wu, Acoustically active lipospheres containing paclitaxel: a new therapeutic ultrasound contrast agent, Invest Radiol, 33 (1998) 886-892.

[14] K. Logan, F. Foglietta, H. Nesbitt, Y. Sheng, T. McKaig, S. Kamila, J. Gao, N. Nomikou, B. Callan, A.P. McHale, J.F. Callan, Targeted chemo-sonodynamic therapy treatment of breast tumours using ultrasound responsive microbubbles loaded with paclitaxel, doxorubicin and Rose Bengal, Eur J Pharm Biopharm, 139 (2019) 224-231.

[15] W. Luo, G. Wen, L. Yang, J. Tang, J. Wang, J. Wang, S. Zhang, L. Zhang, F. Ma, L. Xiao, Y. Wang, Y. Li, Dual-targeted and pH-sensitive Doxorubicin Prodrug-Microbubble Complex with Ultrasound for Tumor Treatment, Theranostics, 7 (2017) 452-465.

[16] Y.J. Bae, Y.I. Yoon, T.J. Yoon, H.J. Lee, Ultrasound-Guided Delivery of siRNA and a Chemotherapeutic Drug by Using Microbubble Complexes: In Vitro and In Vivo Evaluations in a Prostate Cancer Model, Korean J Radiol, 17 (2016) 497-508.

[17] K. Tachibana, S. Tachibana, The use of ultrasound for drug delivery, Echocardiography, 18 (2001) 323-328.

[18] I. Lentacker, S.C. De Smedt, N.N. Sanders, Drug loaded microbubble design for ultrasound triggered delivery, Soft Matter, 5 (2009) 2161-2170.

[19] E. Beguin, S. Shrivastava, N.V. Dezhkunov, A.P. McHale, J.F. Callan, E. Stride, Direct evidence of multibubble sonoluminescence using therapeutic ultrasound and microbubbles, ACS Applied Materials & Interfaces, 11 (2019) 19913-19919.

[20] A. van Wamel, K. Kooiman, M. Harteveld, M. Emmer, F.J. ten Cate, M. Versluis, N. de Jong, Vibrating microbubbles poking individual cells: Drug transfer into cells via sonoporation, Journal of Controlled Release, 112 (2006) 149-155.

[21] G. Dimcevski, S. Kotopoulis, T. Bjånes, D. Hoem, J. Schjøtt, B.T. Gjertsen, M. Biermann, A. Molven, H. Sorbye, E. McCormack, M. Postema, O.H. Gilja, A human clinical trial using ultrasound and microbubbles to enhance gemcitabine treatment of inoperable pancreatic cancer, Journal of Controlled Release, 243 (2016) 172-181.

[22] K. Kusuzaki, H. Murata, T. Matsubara, S. Miyazaki, A. Okamura, M. Seto, A. Matsumine, H. Hosoi, T. Sugimoto, A. Uchida, Clinical trial of photodynamic therapy using acridine orange with/without low dose radiation as new limb salvage modality in musculoskeletal sarcomas, Anticancer Res, 25 (2005) 1225-1235.

[23] L. Freitag, A. Ernst, M. Thomas, R. Prenzel, B. Wahlers, H.N. Macha, Sequential photodynamic therapy (PDT) and high dose brachytherapy for endobronchial tumour control in patients with limited bronchogenic carcinoma, Thorax, 59 (2004) 790-793.

[24] A.P. Castano, T.N. Demidova, M.R. Hamblin, Mechanisms in photodynamic therapy: part one-photosensitizers, photochemistry and cellular localization, Photodiagnosis Photodyn. Ther., 1 (2004) 279-293.

[25] C. McEwan, J. Owen, E. Stride, C. Fowley, H. Nesbitt, D. Cochrane, C.C. Coussios, M. Borden, N. Nomikou, A.P. McHale, J.F. Callan, Oxygen carrying microbubbles for enhanced sonodynamic therapy of hypoxic tumours, J. Control. Release, 203 (2015) 51-56.

[26] V. Kersemans, S. Gilchrist, S. Wallington, P.D. Allen, A.L. Gomes, G.M. Dias, B. Cornelissen, P. Kinchesh, S.C. Smart, A Carbon-Fiber Sheet Resistor for MR-, CT-, SPECT-

, and PET-Compatible Temperature Maintenance in Small Animals, Tomography, 5 (2019) 274-281.

[27] P. Kinchesh, S. Gilchrist, J.S. Beech, A.L. Gomes, V. Kersemans, R.G. Newman, B. Vojnovic, P.D. Allen, M. Brady, R.J. Muschel, S.C. Smart, Prospective gating control for highly efficient cardio-respiratory synchronised short and constant TR MRI in the mouse, Magn Reson Imaging, 53 (2018) 20-27.

[28] V.L. Yarnykh, Actual flip-angle imaging in the pulsed steady state: a method for rapid three-dimensional mapping of the transmitted radiofrequency field, Magn. Reson. Med., 57 (2007) 192-200.

[29] P. Kinchesh, P. Allen, J. Beech, E. Fokas, S. Gilchrist, V. Kersemans, R. Muschel, S. Smart, Dynamic reacquisition for respiratory gated constant TR 2D multi-slice MRI, in: 23rd annual meeting, International Society for Magnetic Resonance in Medicine, 2015.

[30] R Core Team, R: A language and environment for statistical computing, R Foundation for Statistical Computing, Vienna, Austria (2020) in, https://www.R-project.org/.

[31] J.Y. Lee, M.S. Kim, E.H. Kim, N. Chung, Y.K. Jeong, Retrospective growth kinetics and radiosensitivity analysis of various human xenograft models, Lab Anim Res, 32 (2016) 187-193.

[32] Y. Shibamoto, O. Ike, H. Mizuno, T. Fukuse, S. Hitomi, M. Takahashi, Proliferative activity and micronucleus frequency after radiation of lung cancer cells as assessed by the cytokinesis-block method and their relationship to clinical outcome, Clin Cancer Res, 4 (1998) 677-682.

[33] N. Ishibashi, T. Maebayashi, T. Aizawa, M. Sakaguchi, H. Nishimaki, S. Masuda, Correlation between the Ki-67 proliferation index and response to radiation therapy in small cell lung cancer, Radiat Oncol, 12 (2017) 16.

[34] C.S. Wegner, J.-V. Gaustad, L.M.K. Andersen, T.G. Simonsen, E.K. Rofstad, Diffusion-weighted and dynamic contrast-enhanced MRI of pancreatic adenocarcinoma xenografts: associations with tumor differentiation and collagen content, Journal of Translational Medicine, 14 (2016) 161.

[35] R. Klaassen, A. Steins, O.J. Gurney-Champion, M.F. Bijlsma, G. van Tienhoven, M.R.W. Engelbrecht, C.H.J. van Eijck, M. Suker, J.W. Wilmink, M.G. Besselink, O.R. Busch, O.J. de Boer, M.J. van de Vijver, G.K.J. Hooijer, J. Verheij, J. Stoker, A.J. Nederveen, H.W.M. van Laarhoven, Pathological validation and prognostic potential of quantitative MRI in the characterization of pancreas cancer: preliminary experience, Mol Oncol, 14 (2020) 2176-2189.